Formation of the Fe₂Al₅ Intermetallic Phase and Its Effect on Microstructure and Properties in Al–Fe PM Sinters

M. Majchrowska * (ID)**, M. Nowak**
AGH University of Science and Technology, Poland
* Correspondence contact: e-mail: susniak@agh.edu.pl

Abstract

This study investigates the formation and influence of the Fe₂Al₅ intermetallic phase in Al–Fe sintered composites produced via solid-state powder metallurgy. Aluminium–iron powder mixtures containing 25, 29, and 34 at.% Fe were compacted under a pressure of 400 MPa and vacuum-sintered at 580 °C. Microstructural characterisation was performed using scanning electron microscopy (SEM), energy-dispersive X-ray spectroscopy (EDS), and X-ray diffraction (XRD). Image analysis confirmed the presence of three distinct regions: an aluminium matrix, Fe-rich zones, and a newly formed η-phase (Fe₂Al₅). The formation of the Fe₂Al₅ phase was observed locally at the interfaces between the aluminium matrix and iron particles, as a result of solid-state diffusion during sintering. The growth direction of this phase suggests that aluminium diffused into iron, resulting in the formation of reaction layers characteristic of aluminium-rich compositions. XRD analysis revealed no detectable peaks corresponding to FeAl₃ or FeAl₂ phases, confirming that intermetallic phase evolution proceeded entirely in the solid state. Microhardness measurements showed significantly elevated values in Fe₂Al₅-rich regions, highlighting its strengthening potential. The results confirm that Fe₂Al₅ can be effectively synthesised via solid-state diffusion, without liquid phase formation. This approach enables the controlled development of intermetallic phases in Al–Fe systems and offers promising prospects for low-temperature manufacturing of materials with improved mechanical properties.

Keywords: Al–Fe system, Intermetallic phases, Fe₂Al₅, Powder metallurgy

1. Introduction

Intermetallic phases formed in the Al–Fe system are known to strongly affect the mechanical properties and integrity of metal matrix composites produced by powder metallurgy. Depending on the local chemical composition, microstructure, and thermal history, various phases such as Fe₃Al, FeAl, FeAl₂, Fe₂Al₅, and FeAl₃ may form, each distinct structural features, thermodynamic stability, and deformation behavior [1–4]. Among these, Fe₂Al₅ (η-phase) frequently develops at the interface between aluminium matrix and iron particles, especially under conditions promoting solid-state diffusion. The formation of such phases is influenced by the asymmetry of atomic mobility in the Al–Fe system, where aluminium diffuses more readily into iron, leading to the growth of reaction layers [5–7]. This behavior has also been observed in Al–Fe composites produced by powder metallurgy with high-pressure consolidation, where the Fe₂Al₅ phase was identified at the interfaces [5,8]. Understanding the nucleation and growth of these intermetallics is essential for tailoring the microstructure and mechanical properties of aluminium-based materials. Additionally, mechanical design studies confirm the role of intermetallic phases in controlling strength-to-weight ratios, thermal stability, and failure modes in structural applications [9]. The morphology and

extent of the formed phases can significantly affect the strength, ductility, and hardness of the final composite.

In aluminium-rich compositions with iron additions, intermetallics such as Fe_2Al_5 tend to form locally around Fe particles as thin layers or isolated islands. These phases are observed at the Al–Fe interface in response to local diffusion gradients and limited mutual solubility, especially when sintering is performed below the eutectic temperature [10–12]. The presence of Fe_2Al_5 at the particle boundaries confirms that the reaction proceeds in the solid state, without the involvement of a liquid phase [3,8]. Moreover, powder metallurgy offers a unique advantage in controlling phase formation through precise selection of particle size, stoichiometry, and sintering conditions. Such control enables the development of materials with enhanced interfacial strength and locally reinforced microstructures, as demonstrated in the present study.

To obtain improved mechanical or functional properties, a strong metallurgical bond between Al and Fe is essential. One approach to forming intermetallic phases at lower temperatures is the use of solid-state sintering techniques. Although these phases improve bonding, excessive formation may induce brittleness and deteriorate mechanical performance [2,13]. Powder metallurgy enables precise control of chemical composition, near-net-shape fabrication, and cost-efficient processing [8,9,11]. Review articles confirm that phase formation is governed by thermodynamic parameters, interdiffusion mechanisms, and sintering kinetics in Al–Fe systems processed by PM techniques [14].

Sintering of elemental aluminum and iron powders can result in undesirable swelling and shrinkage due to significant differences in diffusion coefficients and solubility limits. Swelling occurs primarily due to outward Al diffusion during heating—a mechanism exploited utilized in the development of dispersion-strengthened ferrous alloys [11,15]. These dispersions inhibit grain growth at elevated temperatures and improve both creep resistance and oxidation behavior [12,13]. The sintering process of Al–Fe systems has been extensively studied by Lee and German [16], who demonstrated that key parameters such as alloy composition, particle size, green density, heating rate, sintering temperature, and prealloying strongly influence densification and the extent of swelling. Their dilatometric studies provided a detailed explanation of sintering kinetics, highlighting the role of solid-state interdiffusion mechanisms. Additional studies confirmed that Fe–Al interdiffusion plays a dominant role during powder metallurgy processing [6,14]. Liu et al. [7] also noted that Fe_2Al_5 has the lowest formation enthalpy among Fe–Al intermetallics, favouring its formation. These insights are important for interpreting the observed dominance of the η-phase (Fe_2Al_5) and the associated porosity and swelling effects reported in this study.

The formation of Al–Fe intermetallics during powder metallurgy processing has been extensively investigated. Kang and Hu [15] demonstrated that the application of mechanical alloying followed by reactive sintering facilitates the formation of Fe_2Al_5 and $FeAl_3$ phases at relatively low temperatures. Krasnowski et al. [5] showed that both the morphology and volume fraction of intermetallic phases are highly sensitive to the Fe/Al ratio and sintering temperature, particularly in systems rich in aluminium. These findings were supported by Matysik et al. [1], who systematically investigated microstructural evolution and phase formation in Al–Fe composites prepared by powder metallurgy.

The results confirmed the phase formation path in aluminium-rich compositions, indicating the appearance of $FeAl_2$ at 68 at.% Al, Fe_2Al_5 at 72 at.%, and $FeAl_3$ at 77.5 at.% Al. In both studies [1,5], the importance of peritectoid and eutectoid reactions in the Fe–Al system was emphasised. Furthermore, Dudina et al. [13] highlighted the role of mechanical activation and compaction pressure in enhancing the kinetics of intermetallic phase formation in Fe–Al systems processed via powder metallurgy.

Given the complexity of phase formation and the sensitivity of Fe_2Al_5 to process conditions, there is a need for detailed investigation into how composition affects its formation, distribution, and the resulting densification and hardness in sintered Al–Fe systems. Accordingly, this study focuses on analysing the relationship between Fe_2Al_5 phase formation, porosity, and mechanical properties in Al–Fe sinters obtained via powder metallurgy.

2. Materials and Work Methodology

The samples were fabricated using a conventional powder metallurgy route involving the following steps: (i) powder mixing, (ii) cold compaction of the mixed elemental powders, and (iii) vacuum sintering of the green compacts.

2.1. Materials

Commercially pure aluminium (99.5%, Fine-Chem Ltd.) and iron (99.5%, NC100.24, Höganäs) powders were used as starting materials. The aluminium powder (Figure 1), produced by gas atomization, exhibited an irregular particle shape with flattened surfaces, protrusions, and surface indentations, characteristic of atomized powders. The iron powder (Figure 2), supplied by Höganäs, showed a highly porous, sponge-like structure and an irregular morphology, typical of sponge powders obtained by chemical reduction processes.
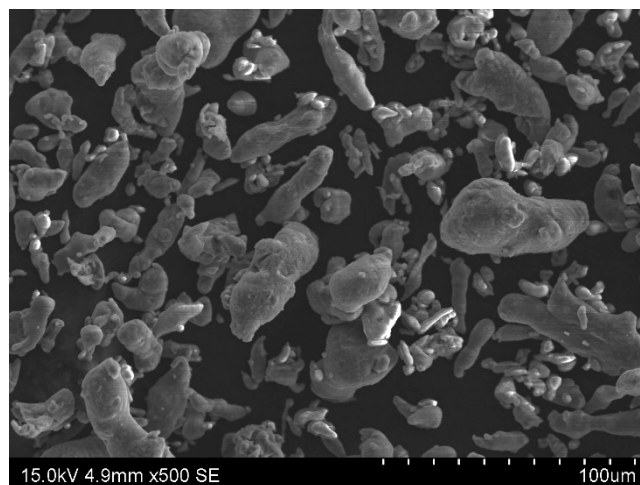

Fig. 1. Morphology of aluminum powder
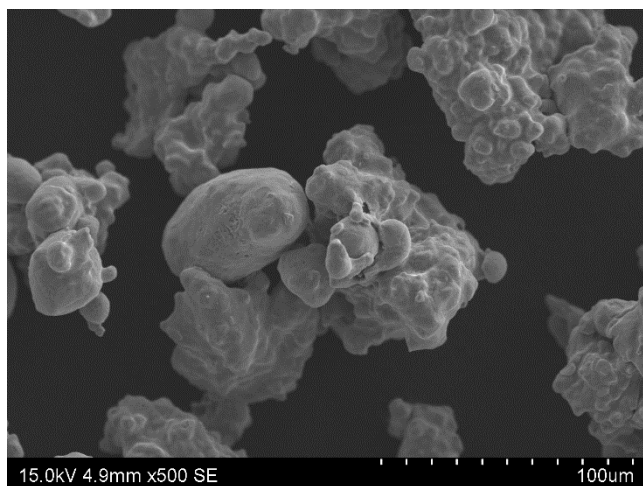
15.0kV 4.9mm x500 SE   100um

Fig. 2. Morphology of iron powder

The significant difference in particle size, combined with the irregular shape and porosity of the Fe particles, was intentionally used to improve packing density. In particular, the smaller aluminium particles effectively filled the voids and intersticles between the larger sponge-like iron particles during mixing. This promoted better particle rearrangement, enhanced powder compaction, and a more uniform distribution of components. The broader particle size distribution of the aluminium powder (Figure 1) further contributed to effective packing and improved interparticle contact, which is advantageous for uniform sintering behavior and intermetallic phase development.

2.2. Preparation of Powder Mixtures and Consolidation

Elemental aluminium and iron powders were weighed in appropriate proportions to produce three powder blends: Composition I – 25 at.% Fe and 75 at.% Al, Composition II – 29 at.% Fe and 71 at.% Al, and Composition III – 34 at.% Fe and 66 at.% Al. These compositions correspond to the stoichiometries of Al-rich intermetallic phases in the Al–Fe system – namely $FeAl_3$ (25 at.% Fe), Fe_2Al_5 (~29 at.% Fe), and $FeAl_2$ (~33 at.% Fe). They were selected to span the compositional range around the Fe_2Al_5 phase, which is known to form preferentially by solid-state diffusion at intermediate temperatures. Maintaining compositions slightly above and below the Fe_2Al_5 stoichiometry enabled the evaluation of dominant and secondary phase formation tendencies: the 25 at.% Fe mixture is slightly Al-rich relative to Fe_2Al_5, while the 34 at.% Fe mixture is slightly Fe-rich. This design allowed assessment of whether a single dominant phase (Fe_2Al_5) would form across all compositions or if secondary phases appear when deviating from the exact stoichiometry of Fe_2Al_5.

To achieve uniform elemental distribution, the aluminium and iron powders were blended for 20 minutes using a Turbula shaker mixer. No grinding media (balls) were added during mixing process to prevent contamination or excessive particle fragmentation. The selected mixing parameters ensured a uniform distribution of both components. Each mixed powder batch was

then consolidated by cold uniaxial pressing. A pressure of 400 MPa was applied to compress the powder into cylindrical pellets of 10 mm diameter and approximately 5 mm height. This compaction step yielded solid green compacts with sufficient mechanical integrity for handling strength and density for sintering.

Sintering was performed in a vacuum furnace to bond the powders and promote intermetallic phase formation. The compacted samples were heated at a controlled rate of 2 °C/min up to 580 °C, held at the temperature for 1 hour, and then allowed to cool freely to room temperature inside the furnace. The entire sintering cycle lasted approximately 6 hours. A vacuum level in the range of 10^{-3}–10^{-5} bar was maintained during heating and dwell to minimise oxidation of the aluminium and iron particles, thus ensuring clean metal surfaces for interdiffusion. Notably, the chosen peak temperature of 580 °C lies below the melting point of aluminium (660 °C), so sintering proceeded entirely in the solid state. This processing route was deliberate: it facilitated gradual diffusion of Al and Fe, and promoted the formation of the Fe_2Al_5 intermetallic phase as the primary product, without any liquid-phase participation. Avoiding melting also suppressed excessive growth of intermetallics and potential element segregation, allowing Fe_2Al_5 to develop *in situ* through diffusion-controlled reactions.

In summary, the powder metallurgy route—cold pressing followed by low-temperature vacuum sintering—was designed to promote the controlled formation of Fe_2Al_5 as the dominant intermetallic phase in the Al–Fe compacts. This methodology yielded dense sintered materials with a microstructure reflecting the initial powder distribution.

2.3. Microstructural and Mechanical Characterization

The characterisation of the sintered Al–Fe samples included density measurements, microstructural observations, phase identification, microhardness testing, and image-based quantification of phase content. These methods enabled a comprehensive evaluation of both the structural and mechanical characteristics of the materials produced via powder metallurgy.

The green and sintered densities were determined using Archimedes' principle, based on mass measurements in air and distilled water. This method provides a reliable estimation of total porosity, including both open and closed pores. Theoretical density for each composition was calculated using the rule of mixtures, based on the atomic fractions and known densities of aluminium and iron. Relative density was then determined as the ratio of the measured density to the theoretical density.

The microstructure was examined using scanning electron microscopy (SEM, HITACHI S-3400N), operated in both secondary electron (SE) and backscattered electron (BSE) modes, providing information on particle distribution, intermetallic phase morphology, and porosity contrast. Prior to imaging, the specimens were ground, polished and etched to reveal phase boundaries. Chemical composition was analysed using energy-dispersive X-ray spectroscopy (EDS), with point and area analyses performed across intermetallic zones and matrix regions.

X-ray diffraction (XRD) analysis was conducted using a Bruker D8 Advance diffractometer equipped with a Cu $K\alpha_1$ source

(λ = 1.5406 Å). A nickel filter was applied to ensure monochromatic radiation. The scan step size was 0.02°, and the resulting diffractograms were interpreted using the PDF-2 crystallographic database. This allowed identification of phases such as Fe_2Al_5 and FeAl, depending on the iron content in the samples.

Microhardness was measured using the Vickers indentation technique (SHIMADZU HMV-2T E), with a load of 0.1 kgf, a dwell time of 15 seconds, and 10 indentations per sample. Measurements were performed within distinct microstructural zones to distinguish between matrix and intermetallic hardness. The highest hardness values were recorded in intermetallic areas, particularly those rich in Fe_2Al_5, while lower values were observed in the aluminium matrix.

To estimate the volume fractions of individual microstructural constituents, binary image analysis was carried out on SEM micrographs using threshold segmentation in MATLAB. The images were processed to distinguish four distinct regions: Fe_2Al_5 intermetallic phase, Fe-rich areas, aluminium matrix, and pores. Segmentation was based on grayscale intensity and morphological features. Comprehensive segmentation maps were generated for each composition to support quantitative microstructural evaluation.

3. Results and Discussion

3.1. Microstructure observation and phase composition

Observations performed using scanning electron microscopy (SEM) (Figures 3–5, with marked analysis points corresponding to Tables 1–3) revealed three distinct microstructural regions in all compositions: a dark aluminium matrix (point 2 in Tables 1–3, marked as "Al"), bright Fe-rich areas (point 1, marked as "Fe"), and intermediate grey regions corresponding to the newly formed η-phase Fe_2Al_5 (point 3, marked as "Fe_2Al_5"). Points 1, 2, and 3, marked in each SEM image (Figures 3–5), indicate the locations of EDS spot analysis and correspond to Fe-rich regions, the Al matrix, and the Fe_2Al_5 intermetallic phase, respectively.

Energy-dispersive spectroscopy (EDS) confirmed a local composition of approximately 72 at.% Al and 28 at.% Fe, which corresponds to the stoichiometry of the Fe_2Al_5 intermetallic phase. This phase was detected in all three compositions, and its dominance is consistent with its low formation enthalpy (–41 kJ/mol) [1,9] and the broad stability range reported in the Al–Fe binary phase diagram [17]. The formation of Fe_2Al_5 at 580 °C, without the involvement of a liquid phase, confirms the effectiveness of solid-state sintering under the applied conditions [2,4,16].

In all compositions (Figures 3–5), rectangular markers indicate Kirkendall-type porosity and interfacial microcracks within the Fe_2Al_5 regions, while arrows indicate additional porous areas. The marked areas represent selected examples and do not reflect the full extent or spatial distribution of porosity or interfacial cracking within the microstructure. These defects, absent in the Fe- or Al-

rich regions, suggest unequal diffusion rates during the solid-state sintering process [11,13].
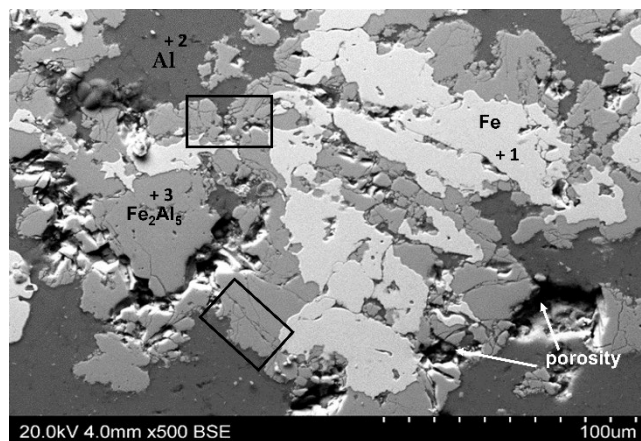

Fig. 3. Microstructure (SEM) of sintered composition I (25 at.% Fe) with point composition analysis

This phenomenon is typical of diffusion-controlled intermetallic growth in the Fe–Al system and is associated with stress concentrations and the inherent brittleness of the intermetallic phase. These findings support the hypothesis that the η-phase is particularly prone to interfacial decohesion, likely due to its complex and anisotropic orthorhombic structure (space group Cmcm), which features a compositionally asymmetric atomic arrangement with partially occupied Al sites, as characterised in detail by Takata et al.[18].

Table 1.
Chemical composition from EDS point analysis (see Figure 3) and corresponding phase identification

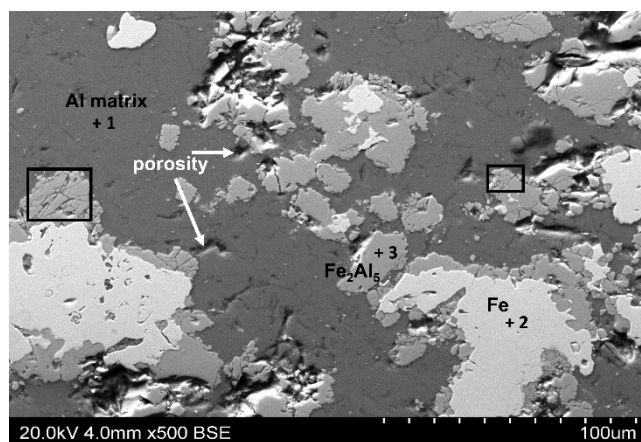| Point No.	Identified Phase (label used in Fig. 3)	Al [at. %]	Fe [at. %]
1	Fe (iron-rich phase)	0.00	100.00
2	Al (aluminium matrix)	99.42	0.58
3	Fe_2Al_5 (intermetallic)	72.60	27.40

Fig. 4. Microstructure (SEM) of sintered composition II (29 at.% Fe) with point composition analysis

Table 2.
Chemical composition from EDS point analysis (see Figure 4) and corresponding phase identification

Point No.	Identified Phase (label used in Fig. 4)	Al [at.%]	Fe [at.%]
1	Fe (iron-rich phase)	1.26	98.74
2	Al (aluminium matrix)	99.48	0.52
3	Fe_2Al_5 (intermetallic)	72.52	27.41

Table 3.
Chemical composition from EDS point analysis (see Figure 5) and corresponding phase identification

Point No.	Identified Phase (label used in Fig. 5)	Al [at. %]	Fe [at. %]
1	Fe (iron-rich phase)	1.44	98.56
2	Al (aluminium matrix)	99.44	0.56
3	Fe_2Al_5 (intermetallic)	71.07	28.93
4	FeAl (intermetallic)	49.17	50.83

Furthermore, in the sample with 34 at.% Fe, the FeAl phase was identified based on both EDS measurements (point 4 in Table 3, marked as FeAl in Figure 5) and XRD analysis (see Section 3.2). In this composition, an additional EDS analysis point (4) was included to identify the FeAl phase, as shown in Figure 5. Its occurrence suggests a possible transition towards more symmetric diffusion conditions at elevated iron concentrations, consistent with findings by Lee and German [16], who demonstrated that increasing Fe content favours the formation of B2-ordered FeAl due to enhanced Al diffusion into Fe-rich areas.

Another interpretation may stem from the morphological characteristics of the iron powder used. The Fe particles exhibited a sponge-like structure with a large internal surface area—typical of powders produced by Höganäs. This morphology may have led to the encapsulation of fine Al particles during mixing and compaction, resulting in locally non-equilibrium regions with Fe excess and restricted Al diffusion. These areas could promote FeAl formation during early sintering, even though Fe_2Al_5 remains the thermodynamically preferred product. This interpretation highlights the interplay between global thermodynamic conditions and local kinetic factors, a concept discussed in recent studies on non-equilibrium sintering and diffusion heterogeneity in Al–Fe systems [11,15,19].
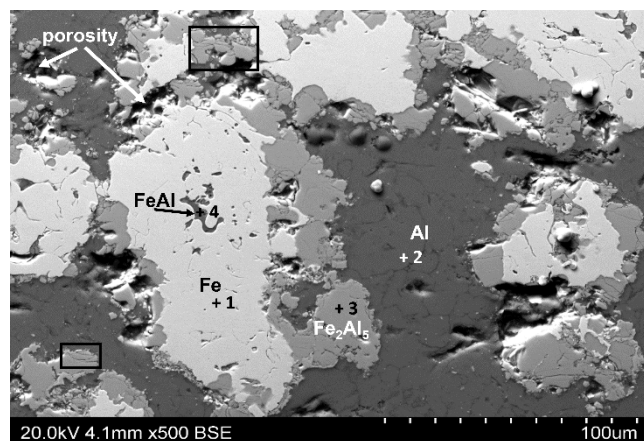
A quantitative evaluation of the Fe_2Al_5 phase fraction was performed based on binary SEM image analysis using MATLAB. The region analysed in Figure 6 corresponds to the microstructure of composition III, previously shown in Figure 5. (composition III). The results, presented in Table 4, show the following contents: 38.32% in composition I (25 at.% Fe), 25.06% in composition II (29 at.% Fe), and 24.85% in composition III (34 at.% Fe). These results confirm that Fe_2Al_5 is the predominant intermetallic phase formed through solid-state diffusion. However, the relationship between Fe content and Fe_2Al_5 volume fraction was nonlinear, reflecting the influence of local diffusion kinetics and phase equilibrium boundaries.

Despite the higher Fe concentration in composition II, the Fe_2Al_5 volume fraction was lower than in composition I. This observation can be explained by the Al–Fe binary phase diagram: composition I (25 at.% Fe) lies well within the Al + Fe_2Al_5 two-phase region, favouring exclusive η-phase formation. In contrast, composition II (29 at.% Fe) is near the boundary between Al + Fe_2Al_5 and Fe_2Al_5 + FeAl, where secondary Fe-rich phases may form locally, limiting further growth of Fe_2Al_5. In composition III (34 at.% Fe), FeAl was identified, as confirmed by EDS (Table 3, point 4) and XRD results (Figure 7), further reducing the amount of Fe_2Al_5 in the final structure.

Fig. 5. SEM micrograph (BSE) of sintered composition III (34 at.% Fe), with marked points for EDS analysis
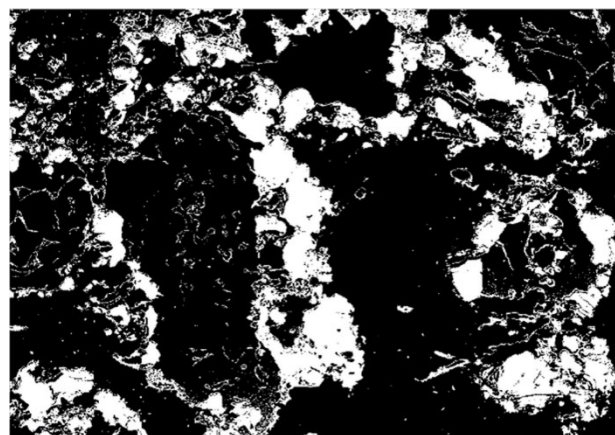

Fig. 6. Representative binary SEM image of composition III (34 at.% Fe), processed using MATLAB for quantitative analysis. Intermetallic regions are shown in white

Table 4.
Volume fraction of different regions in sintered samples based on MATLAB image analysis

Composition	Fe_2Al_5 phase [%]	Al content [%]	Fe content [%]	Porosity [%]
I	38.320	32.570	24.637	4.473
II	25.064	35.209	35.030	3.852
III	24.845	31.092	42.542	1.732

This analysis aligns with the Al–Fe binary phase diagram, which shows that the stability region of Fe_2Al_5 narrows with increasing Fe content. The formation of competing intermetallic, such as FeAl, is increasingly favoured at higher Fe concentrations, especially under non-equilibrium conditions or in cases of asymmetric diffusion, thus limiting the relative fraction of Fe_2Al_5.

3.2. XRD Phase Identification and Structural Interpretation

X-ray diffraction (XRD) analysis (Figure 7) confirmed the formation of Fe_2Al_5 as the dominant intermetallic phase in all sintered compositions. In samples containing 25 at.% and 29 at.% Fe, the diffraction patterns exhibited distinct reflections of Fe_2Al_5, accompanied by residual peaks corresponding to unreacted Fe and Al. In the composition with 34 at.% Fe, additional low-intensity peaks were observed and identified as FeAl, supporting the EDS point analysis from the SEM microstructure (Figure 5). No reflections associated with $FeAl_2$ or $FeAl_3$ were detected, confirming their absence in the investigated samples.

The η-phase Fe_2Al_5 crystallises in an orthorhombic structure (space group Cmcm) with partially occupied Al sites along the c-axis, which introduces atomic disorder and promotes anisotropic growth behavior [7,18]. This crystallographic complexity is a key factor underlying its intrinsic brittleness and limited ductility, which correlate with the interfacial microcracks and decohesion observed in the Fe_2Al_5 zones, particularly at the interfaces with the aluminium matrix, as discussed in Section 3.1 and shown in Figures 3–5.

The repeated identification of Fe_2Al_5 across all compositions supports its high thermodynamic stability and rapid nucleation kinetics, especially under vacuum sintering conditions at moderate temperature (580 °C). These findings are consistent with previous studies by Liu et al. [7], Rabin and Wright [6], and Školáková et al. [19], which demonstrated that solid-state diffusion in the Al–Fe system preferentially stabilises Fe_2Al_5, particularly under non-equilibrium sintering conditions and with Al-rich matrices.

The detection of FeAl in the 34 at.% Fe sample suggests a shift toward more symmetric diffusion conditions, which may promote the formation of B2-ordered intermetallic structures in Fe-rich regions, as previously proposed by Lee and German [16]. This interpretation aligns with the EDS data (Table 3, point 4) and highlights the role of overall composition and local environment on intermetallic phase evolution.
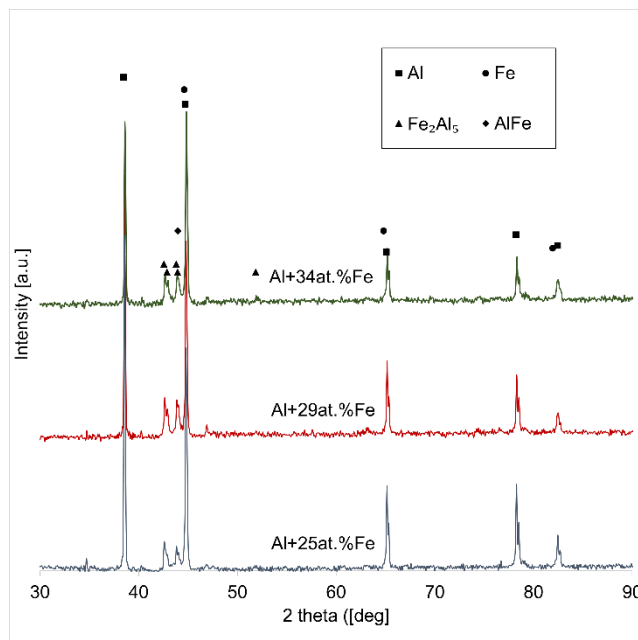

Fig. 7. X-ray diffraction patterns for Al–Fe samples with 25, 29, and 34 at.% Fe recorded after the consolidation process

The structural information obtained from XRD correlates strongly with the SEM/EDS observations, further confirming that Fe_2Al_5 is the primary intermetallic product of solid-state diffusion in the Al–Fe system, with FeAl emerging only at higher Fe concentrations. These insights reinforce the notion that both global composition and local kinetic constraints dictate the phase composition in sintered Al–Fe compacts produced by powder metallurgy.

3.3 Densification and Porosity Evaluation

For the green compacts, the porosity values were as follows: 11.67% for the 25 at.% Fe composition, 11.24% for 29 at.% Fe, and 11.08% for 34 at.% Fe. After sintering, porosity decreased to 9.97%, 9.65%, and 9.25%, respectively, indicating densification. These results suggest that increasing iron content enhances densification due to the higher density of Fe compared to Al, thereby improving packing efficiency and reducing residual porosity (Figure 8).

In addition, local porosity was estimated from microstructural cross-sections using binary SEM image analysis in MATLAB. This method yielded lower porosity values: 4.47%, 3.85%, and 1.73% for the respective compositions corresponding to 25, 29, and 34 at.% Fe. However, SEM-based image analysis is known to underestimate the total porosity, as it captures only surface-connected or visible voids and omits enclosed or subsurface defects. This technique was applied as a complementary approach to characterise near-surface features and to correlate local porosity with the morphology and distribution of intermetallic phases.
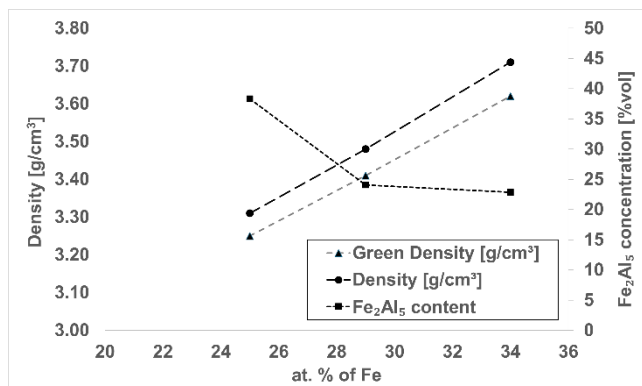
Fig. 8. Green density, sintered density, and Fe_2Al_5 volume fraction in Al–Fe samples with 25, 29, and 34 at.% Fe

The densification behaviour was analysed in relation to Fe content and Fe_2Al_5 phase formation. As shown in Figure 8, both green and sintered densities increased with the overall Fe content due to the inherently higher density of Fe compared to Al. However, an inverse correlation was observed between the Fe_2Al_5 phase fraction and final sintered density. The sample with 25 at.% of Fe, containing the highest volume fraction of Fe_2Al_5 (38.32%), showed the lowest sintered density (3.31 g/cm³), whereas the 34 at.% Fe composition, with the lowest Fe_2Al_5 content (24.85%), demonstrated the highest density (3,70 g/cm³).

This nonlinear trend indicates that densification cannot be fully explained by Fe content alone. While green and sintered densities increased numerically with Fe content, the relative densities—calculated as the ratio of measured to theoretical values—showed a moderate improvement: from 89.8% for the 25 at.% Fe sample, to 90.2% for 29 at.%, and 90.8% for 34 at.%. This confirms that the densification efficiency, rather than the absolute density, improved slightly with Fe addition.

However, the densification gain was partially offset by the increasing formation of the Fe_2Al_5 phase, which has an intrinsic density of approximately 4.2 g/cm³—lower than that of elemental Fe (~7.9 g/cm³). Moreover, the accumulation of Kirkendall-type porosity and microcracking at Fe_2Al_5/Al interfaces likely disrupted full consolidation, limiting the net increase in relative density. These observations highlight that actual phase composition and microstructural integrity, rather than total Fe content, are the primary drivers of densification behaviour.

In contrast, compositions containing a more balanced distribution of phases—including FeAl—achieved improved compaction efficiency, likely due to better diffusion symmetry and reduced interface brittleness as observed in the 34 at.% Fe sample. The presence of heavier residual Fe or FeAl phases, which have higher densities than Fe_2Al_5, may also contribute to the improved densification observed at higher Fe contents.

3.4. Microhardness

Microhardness measurements were performed across all microstructural zones to assess local variations in mechanical properties, with results summarised in Figure 9. The highest values were consistently recorded in regions rich in Fe_2Al_5, ranging from approximately 780 to 870 $HV_{0.01}$, depending on composition. These results confirm the significant hardening contribution of the Fe_2Al_5 phase, which aligns with its documented brittleness, orthorhombic crystal structure, and limited plasticity [1,5,12].

The hardness of the Fe-rich regions remained relatively stable across compositions (~90 $HV_{0.01}$), while that of the aluminium matrix was significantly lower (~40–50 $HV_{0.01}$), reflecting the soft nature of pure Al. Notably, a slight increase in Fe_2Al_5 microhardness was observed in the 34 at.% Fe sample, which may be attributed to greater phase continuity and a reduced fraction of the ductile Al matrix.

Despite the locally high hardness, a slight reduction in overall mechanical integrity was noted with increasing Fe content. This reduction is most likely caused by increased microcrack density and interfacial Kirkendall porosity at Fe_2Al_5–Al boundaries, which act as stress concentrators [11,13]. These mechanisms have been discussed in detail in Section 3.1 and are well documented in the context of diffusion-controlled intermetallic interfaces in Al–Fe systems.

Moreover, the presence of numerous Fe_2Al_5/Al interfaces may contribute to increased macroscopic brittleness, especially under cyclic or impact loading conditions, where crack initiation and propagation are facilitated by the anisotropic crystal structure and low ductility of the η-phase [5,12]. Similar trends were previously reported by Fathy et al. [20], who observed that an increased fraction of Fe_2Al_5 intermetallics in Fe–Al PM compacts led to higher hardness but also reduced ductility due to brittle phase morphology and the formation of microcracks.
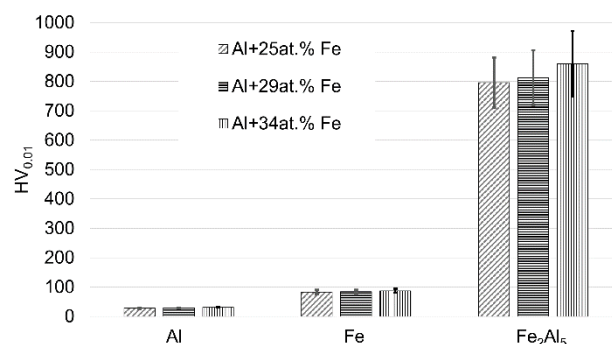

Fig. 9. Vickers microhardness of the sintered samples in different areas: aluminium, iron, and Fe_2Al_5 intermetallic

The heterogeneous distribution of microhardness values highlights the critical role of microstructural control, particularly in terms of phase formation and residual porosity, in achieving balanced mechanical properties. The data presented in Figure 9 illustrate that, while Fe_2Al_5 contributes to local strengthening, its excessive formation may compromise overall cohesion and ductility of the sintered material.

4. Conclusions

The present study has demonstrated that intermetallic compounds in the Al–Fe system can be effectively synthesised via solid-state powder metallurgy using elemental powders, cold

compaction at 400 MPa, and vacuum sintering at 580 °C. The results provide valuable insights into the mechanisms of phase formation, porosity characteristics, and the mechanical response in Al–Fe sintered compacts.

The η-phase Fe_2Al_5 was identified as the predominant intermetallic phase in all compositions, which is in accordance with thermodynamic predictions and was confirmed by XRD and EDS analyses. In the sample containing 34 at.% Fe, the formation of an additional FeAl phase was observed, which may be attributed to changes in diffusion dynamics at elevated iron concentrations.

Microstructural observations revealed Kirkendall-type porosity and interfacial microcracks, particularly at the Fe_2Al_5/Al boundaries. These defects, attributed to differences in atomic mobility during diffusion, were more pronounced in compositions with higher Fe_2Al_5 content and were correlated with a lower densification efficiency.

Porosity was analysed using two complementary methods: the Archimedes method, based on mass measurements in air and water, and SEM image analysis performed in MATLAB. The Archimedes method enabled accurate quantification of total porosity, including both open and closed pores, while SEM-based image analysis provided insight into local internal porosity. The difference between the methods highlighted the importance of considering surface-connected and closed defects in densification studies.

Despite the expected densification effect of increasing Fe content, a nonlinear relationship was observed between total Fe concentration and sintered density. This outcome reflects the complex interplay between chemical composition and phase distribution: while Fe itself is dense, the formation of intermetallic phases such as Fe_2Al_5—characterised by lower mass density—may locally limit densification. Moreover, the associated formation of Kirkendall-type porosity and interfacial microcracks further impedes compaction. These results emphasise that actual phase morphology and microstructural integrity, rather than nominal Fe content alone, are decisive factors in densification efficiency.

Microhardness measurements revealed significantly elevated hardness in Fe_2Al_5-rich regions (780–870 $HV_{0.01}$), confirming the strong hardening effect of this intermetallic phase. The non-uniform distribution of hardness within the microstructure highlights the critical importance of phase formation control and porosity reduction in achieving uniform mechanical performance.

Overall, the findings confirm that low-temperature solid-state sintering is a viable and energy-efficient route for synthesising Al–Fe intermetallic materials without liquid phase formation. The balance between intermetallic phase evolution and densification remains a key parameter for tailoring microstructure and mechanical performance in Al–Fe powder metallurgy systems.

Acknowledgements

References

[1] Matysik, P., Jóźwiak, S., & Czujko, T. (2015). Characterization of low-symmetry structures from phase equilibrium of Fe–Al system—Microstructures and mechanical properties. *Materials.* 8(3), 914-931. https://doi.org/10.3390/ma8030914.

[2] Šesták, P., Friák, M., Holec, D., Všianská, M. & Šob, M. (2018). Strength and brittleness of interfaces in Fe–Al superalloy nanocomposites under multiaxial loading: An ab initio and atomistic study. *Nanomaterials.* 8(11), 873, 1-20. https://doi.org/10.3390/nano8110873.

[3] Zhang Y., Zhao T., Yu X. & Huang J. (2023). The Al-Fe intermetallic compounds and the atomic diffusion behavior at the interface of aluminum-steel welded joint. *Metals.* 13(2), 334, 1-14. https://doi.org/10.3390/met13020334.

[4] Wang, Q., Leng, X.S., Yang, T.H. & Yan, J.C. (2014). Effects of Fe–Al intermetallic compounds on interfacial bonding of clad materials. *Transactions of Nonferrous Metals Society of China.* 24(1), 279-284. https://doi.org/10.1016/S1003-6326(14)63058-2.

[5] Krasnowski, M., Gierlotka, S. & Kulik, T. (2016). Nanocrystalline Al_5Fe_2 intermetallic and Al_5Fe_2–Al composites manufactured by high-pressure consolidation of milled powders. *Journal of Alloys and Compounds.* 656, 82-87. https://doi.org/10.1016/j.jallcom.2015.09.224.

[6] Rabin, B.H. & Wright, R.N. (1991). Synthesis of iron–aluminides from elemental powders: Reaction mechanisms and densification behavior. *Metallurgical Transactions A.* 22A, 277-286. https://doi.org/10.1007/BF02656797.

[7] Liu, Y., Chong, X., Jiang, Y., Zhou, R. & Feng, J. (2017). Mechanical properties and electronic structures of Fe–Al intermetallic. *Physica B: Condensed Matter.* 506, 1-11. https://doi.org/10.1016/j.physb.2016.10.032.

[8] Karwan-Baczewska, J., Dymkowski, T. & Seetharaman, S. (2000). Manufacturing of intermetallic alloys by conventional powder metallurgy technology and thermochemical treatment. *Archives of Metallurgy.* 45(3), 261-275.

[9] Ashby, M.F. (2005). *Materials Selection in Mechanical Design.* (3rd ed.). Burlington, MA, USA: Butterworth-Heinemann.

[10] Novák, P., Knotek, V., Šerák, J., Michalcová, A. & Vojtěch, D. (2011). Synthesis of Fe–Al–Si intermediary phases by reactive sintering. *Powder Metallurgy.* 54(2), 167-171. https://doi.org/10.1179/174329009X449314.

[11] Kim, Y.I., Lee, W., Jang, J.M., Ui, S.W., An, G.S., Kwon, H. & Ko, S.H. (2018). Effects of aluminum content and particle size on volume expansion during the sintering of Fe–Al mixed powders. *Journal of Alloys and Compounds.* 747, 211-216. https://doi.org/10.1016/j.jallcom.2018.02.299.

[12] Silvayeh, Z., Götzinger, B., Karner, W., Hartmann, M. & Sommitsch, C. (2018). Calculation of the intermetallic layer thickness in cold metal transfer welding of aluminum to steel. *Materials.* 12(1), 35, 1-16. https://doi.org/10.3390/ma12010035.

[13] Dudina, D.V., Legan, M.A., Fedorova, N.V., Novoselov, A.N., Anisimov, A.G. & Esikov, M.A. (2017). Structural and mechanical characterization of porous iron aluminide FeAl obtained by pressureless spark plasma sintering. *Materials*

Science and Engineering A. 695, 309-314. http://dx.doi.org/10.1016/j.msea.2017.04.051.

[14] Que, Z., Wang, Y., Mendis, C. L., Fang, C., Xia, J., Zhou, X., & Fan, Z. (2022). Understanding Fe-Containing intermetallic compounds in Al alloys: An overview of recent advances from the LiME Research Hub. *Metals.* 12(10), 1677, 1-33. https://doi.org/10.3390/met12101677.

[15] Kang, H.Z. & Hu, C.T. (2004). Swelling behavior in reactive sintering of Fe–Al mixtures. *Materials Chemistry and Physics.* 88(2-3), 264-272. https://doi.org/10.1016/j.matchemphys.2004.03.001.

[16] Lee, D.J. & German, R.M. (1985). Sintering behavior of iron–aluminium powder mixes. *International Journal of Powder Metallurgy.* 21, 9-21.

[17] Murray, J.L. (1992). Fe–Al binary phase diagram. In: H. Baker (Eds.), *Alloy Phase Diagrams* (p. 54). Materials Park, OH, USA: ASM International.

[18] Takata, N., Nishimoto, M., Kobayashi, S. & Takeyama, M. (2015). Crystallography of Fe_2Al_5 phase at the interface between solid Fe and liquid Al. *Intermetallics.* 67, 1-11. https://doi.org/10.1016/j.intermet.2015.07.011.

[19] Školáková, A., Pinc, J. & Novák, P. (2022). The preferential formation of Ni_2Al_3, Fe_2Al_5, and Ti_2Al_5 phases in aluminide systems. *Materials Chemistry and Physics.* 280, 125859, 1-5. https://doi.org/10.1016/j.matchemphys.2022.125859.

[20] Durejko, T. (2016). Structure and properties of the Fe_3Al-type intermetallic alloys fabricated by powder metallurgy. *Materials Science and Engineering: A.* 674, 1–9. https://doi.org/10.1016/j.msea.2016.08.060.